PLANTRSR: A NEW PLANT DATASET AND METHOD FOR REFERENCE-BASED SUPER-RESOLUTION

Hongyang Zhou[1], **Xiaobin Zhu**[1]*, **Shengxiang Yu**[2*], **Liuling Chen**[1], **Jingyan Qin**[1], **Xu-Cheng Yin**[1]
[1]University Of Science and Technology Beijing,
[2]Institute of Botany, Chinese Academy of Sciences

ABSTRACT

Single image super-resolution (SISR) often struggles to reconstruct high-resolution (HR) details from heavily degraded low-resolution (LR) inputs. Instead, reference-based super-resolution (RefSR) methods offer an alternative solution to generate promising results using high-quality reference (Ref) images to guide reconstruction. However, existing RefSR datasets focus on limited scene types, primarily featuring human activities and architectural scenes. Plant scenes exhibit complex textures and fine details, essential for advancing RefSR in natural and highly detailed scenes. To this end, we meticulously captured and manually selected high-quality images containing rich textures to construct a large-scale plant dataset, **PlantRSR**, comprising 16,585 HR–Ref pairs. The dataset captures the complexity and variability of plant scenes through extensive variations. In addition, we propose a novel RefSR method specifically designed to tackle the distinct challenges posed by plant imagery. It incorporates a Selective Key-Region Matching (SKRM) that selectively identifies and performs matching between LR and Ref images, focusing on distinctive botanical textures to improve matching efficiency. Additionally, a Texture-Guided Diffusion Module (TGDM) is proposed to refine LR textures by leveraging a diffusion process conditioned on the matched Ref textures. TGDM is effective in modeling irregular and fine textures, thereby facilitating more accurate SR results. The proposed method achieves significant improvements over state-of-the-art (SOTA) approaches on our PlantRSR dataset and other benchmarks. Code and dataset are released at:`https://github.com/edbca/PlantRSR`.

1 INTRODUCTION

SISR aims to reconstruct an HR image from an LR input, and has been widely applied in various fields, including critical uses in plant phenotyping, where high-resolution imagery is crucial for detailed morphological analysis, disease diagnosis, and growth monitoring in precision agriculture. While SISR has shown promising results Dai et al. (2019); Niu et al. (2020); Huang et al. (2021); Kong et al. (2021); Wang et al. (2021); Zhou et al. (2023); Wang et al. (2024a); Guo et al. (2025), it often fails to reconstruct precisely detailed textures of the ground-truth HR image when the original high-frequency information is severely lost during the degradation. To address this issue, RefSR methods Zhang et al. (2019); Yang et al. (2020); Lu et al. (2021); Jiang et al. (2021); Xia et al. (2022); Cao et al. (2022); Zhou et al. (2025) incorporates external Ref images as guidance, leveraging external high-quality textural details to enhance texture recovery.

Recent RefSR methods leverage feature alignment, attention mechanisms, or implicit correspondence learning to fuse textures from Ref images. Despite significant progress, existing studies primarily focus on limited scenes such as human daily life and architectural structures, as reflected by datasets like CUFED5 Zhang et al. (2019) and LMR Zhang et al. (2023). As shown in Fig. 1 (a) and (b), CUFED5 and LMR mainly contain scenes with rigid structures and limited geometric variations. In contrast, plant scenes, as shown in Fig. 1 (c), exhibit distinct characteristics such as significant shape deformation, subtle texture variations, and frequent defocused backgrounds, which introduce

[*]Xiaobin Zhu and Shengxiang Yu are the corresponding authors.

additional challenges for RefSR. Moreover, the lack of publicly available RefSR datasets tailored to plant imagery restricts the development of methods capable of handling its unique challenges. Although the DRefSR Zhou et al. (2025) expands upon CUFED5 by increasing data diversity and includes certain plant images, it is not specifically designed for plant scenes and suffers from insufficient quantity and variety. As a result, existing approaches often struggle to generalize to such complex and diverse scenarios. In particular, plant imagery presents unique challenges, such as irregular structures and diverse textures, that differ significantly from the relatively structured content found in current datasets. This highlights the necessity for RefSR datasets and strategies specifically tailored to plant imagery.

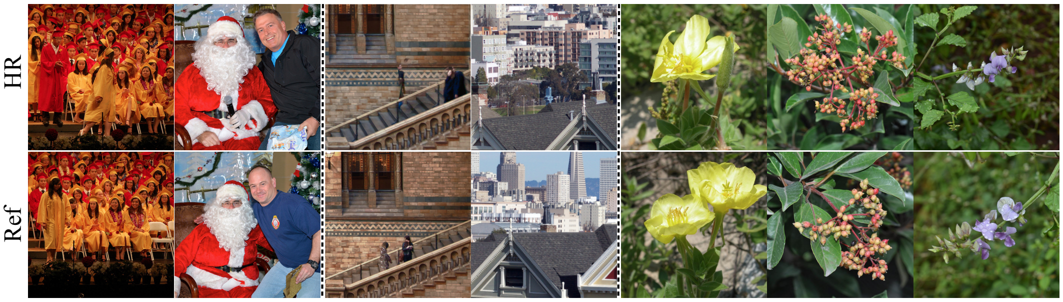

(a) CUFED5 dataset (b) LMR dataset **(c) Our PlantRSR dataset**

Figure 1: Example image pairs from different RefSR datasets. (a) CUFED5 dataset Zhang et al. (2019), primarily featuring scenes of human daily activities. (b) LMR dataset Zhang et al. (2023), focused on architectural scenes. (c) Our PlantRSR dataset, designed for complex botanical textures with diverse plant species.

To address the above challenges, we construct a novel large-scale RefSR dataset specifically designed for plant imagery, named **PlantRSR**. All images were carefully captured by us from real-world plant scenes, ensuring high authenticity and diversity. The dataset comprises 6,134 high-quality HR–Ref image pairs with extensive variations in color, rotation, deformation, and background blur, covering resolutions from 2K to 8K. In RefSR tasks, models are commonly trained using cropped image patches, since full-resolution images are often too large for direct processing. However, generating aligned patch pairs is particularly challenging. Automated patch generation in previous datasets often leads to misaligned or semantically inconsistent pairs, which is unsuitable for complex plant imagery. To ensure high-quality training data, we manually annotate and construct 16,585 semantically aligned HR–Ref patch pairs, exceeding the 11,817 pairs in the widely used CUFED5 dataset. Besides, the PlantRSR dataset includes a testing set of 100 image pairs, offering the first RefSR benchmark for plant imagery and a solid foundation for future research.

We introduce an innovative RefSR approach tailored to address the distinct challenges in plant environments. First, we propose a Selective Key-Region Matching (SKRM) that can target the focal characteristics of plant images, performing matching only on key regions between LR and Ref images to significantly enhance matching efficiency. Second, we present a Texture-Guided Diffusion Module (TGDM), which enhances LR features by incorporating matched Ref textures as conditional guidance within a diffusion-based refinement framework. This novel module effectively leverages the fine-grained and irregular textures from the Ref image to improve the quality of the SR image. Together, these components form a unified framework that ensures both accurate texture transfer and efficient feature enhancement. Extensive experiments demonstrate the superiority of our method. In summary, our main contributions are four-fold:

- We contribute a new large-scale plant dataset for RefSR, named PlantRSR, which contains 16,585 high-quality training pairs with rich variations in color, rotation, deformation, and background blur, reflecting the complexity of real-world plant scenes.
- We propose a novel RefSR method specifically designed to tackle the challenges posed by plant imagery. Extensive experiments on multiple datasets demonstrate that our method outperforms SOTA methods both quantitatively and qualitatively.
- We propose a Selective Key-Region Matching (SKRM) module that leverages the focal characteristics of plant imagery to perform region-specific matching between LR and Ref images, thereby significantly enhancing matching effectiveness.

- We propose a Texture-Guided Diffusion Module (TGDM) that introduces a diffusion mechanism conditioned on matched Ref textures to refine LR regions, enabling more accurate reconstruction of the SR image.

2 Related Work

Reference-based Image Super-Resolution. Unlike conventional SISR methods that rely exclusively on the LR input, RefSR incorporates an additional high-quality Ref image to supply textures and structural details. Pioneer RefSR methods mainly emphasized alignment between the LR and Ref images. For instance, Wang *et al.* Wang et al. (2016b) proposed iterative non-uniform warping to refine the Ref for better texture extraction. CrossNet Zheng et al. (2018a) employs multi-scale optical flow to achieve spatial alignment, while SSEN Zheng et al. (2018b) adopts deformable convolutions (Dai et al., 2017; Zhu et al., 2019) to align feature representations adaptively.

In addition to alignment-based strategies, a significant body of work has explored patch-based texture transfer. SRNTT Zhang et al. (2019), for example, utilizes perceptual features extracted from VGG Simonyan & Zisserman (2015) to identify semantically similar textures between LR and Ref images. E2ENT2 Xie et al. (2020) proposes a task-specific feature extraction framework, moving beyond general classification features. TTSR Yang et al. (2020) designs a cross-scale transformer to effectively aggregate textures across multiple levels. Other approaches, such as AMRSR Pesavento et al. (2021) and CIMR-SR Yan et al. (2020), expand to multi-Ref settings for richer texture guidance. MASA Lu et al. (2021) addresses efficiency through a hierarchical coarse-to-fine matching scheme. To tackle domain discrepancies in resolution and content, C^2-Matching Jiang et al. (2021) introduces contrastive learning He et al. (2020) and knowledge distillation Hinton (2015) for robust correspondence learning. At the same time, DATSR Cao et al. (2022) leverages transformer architectures for better handling of scale and transformation variations. RRSR Zhang et al. (2022) proposes a reciprocal mechanism where reconstruction feedback enhances the overall performance. Ref-IRT Zhang et al. (2024) introduces a progressive restoration pipeline for handling complex degradations. MCMSR Zheng et al. (2024) focuses on discovering multiple matching candidates in the Ref image for each LR region to improve completeness. SSMTF Zhou et al. (2025) attempts to leverage state-space models to extract multi-scale information from Ref images. Recently, diffusion models have emerged as a powerful paradigm for leveraging Ref information. DiffMSR Li et al. (2024a) employs diffusion to generate prior knowledge from Ref for magnetic resonance image reconstruction. Similarly, in remote sensing, Ref-Diff Dong et al. (2024) proposes a change-aware diffusion model to extract change priors from Ref images. CoSeR Sun et al. (2024), instead of using a physical Ref, utilizes a diffusion model to generate a semantically relevant Ref image to aid reconstruction. This idea of *generating* references connects to retrieval-augmented methods; for example, RAG Lee et al. (2025) proposes a Retrieval-Augmented Generation framework that retrieves a Ref image given an LR query. However, most existing methods still face limitations in complex scenarios like plant imagery, which features irregular structures and diverse textures that are significantly different from the current dataset.

Datasets for Reference-based Image Super-Resolution. SISR datasets such as DIV2K Timofte et al. (2017) and Flickr2K Lim et al. (2017) have been widely adopted to learn mappings from LR to HR images. However, they are not well-suited for RefSR tasks, as they lack external Ref images that are crucial for guiding texture enhancement Zheng et al. (2018a); Zhang et al. (2019). To bridge this gap, CUFED5 Zhang et al. (2019) is proposed as an early dataset tailored for RefSR, offering 13,761 training pairs of size 160×160, each consisting of a HR image and a corresponding Ref image. CUFED5 provides 126 test groups for evaluation, where each group includes an HR image and four Ref images with varying degrees of similarity. Following this, Lin *et al.* Zhang et al. (2023) introduced the LMR dataset, a large-scale multi-reference benchmark designed to further enrich RefSR research. It comprises 112,142 training groups of 300×300 images, each paired with five Ref images across different similarity levels. The testing set includes 142 groups, where each target image is matched with 2 to 6 Ref images. To address the limited diversity of CUFED5, DRefSR Zhou et al. (2025) extends this dataset by constructing a more varied training set comprising 13,761 image pairs. In addition, other efforts, such as Sun80 Sun & Hays (2012) and WR-SR Jiang et al. (2021) offer testing scenarios more aligned with real-world applications. Sun80 provides 80 natural images with internet-sourced reference sets, while WR-SR contains 100 image pairs featuring references retrieved through web search, encompassing diverse visual categories such as animals and landmarks.

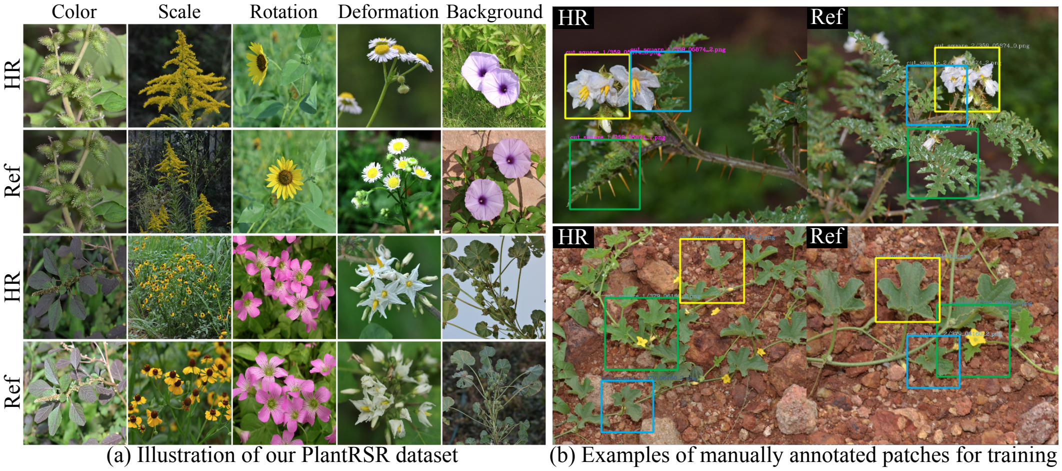

(a) Illustration of our PlantRSR dataset

(b) Examples of manually annotated patches for training

Figure 2: Category overview and training set construction of our PlantRSR dataset.

Despite recent progress, existing RefSR datasets like CUFED5 and LMR offer limited diversity and are ill-suited for plant phenotyping. Although DRefSR expands the variety of scenes and includes some plant imagery, the quantity and diversity of plant species remain insufficient (Detailed analysis in Appendix C). Plant images pose unique challenges such as large shape deformations, subtle textures, and frequent defocus, which are not well represented in current datasets.

3 PlantRSR Dataset Construction

The widely used CUFED5 dataset is constructed from CUFED Wang et al. (2016a) and primarily targets human daily life scenes. Similarly, the LMR dataset, built upon MegaDepth Li & Snavely (2018), focuses mainly on landmark scenarios. These datasets are not well-suited for plant scenes. Furthermore, existing plant-specific datasets remain scarce, making it challenging to obtain valid HR-Ref image pairs. To meet the needs of current RefSR tasks, we meticulously captured 6,134 image pairs with rich textures using DSLR cameras. The images cover resolutions between 2K and 8K, over 80% of which are above 4K. To ensure the diversity and realism of the dataset, we deliberately captured images that reflect five major types of variations commonly encountered in real-world plant photography: color variations (11.4%), scale differences (18.6%), rotations (27.0%), deformations (30.5%), and background changes (12.5%). These variations are introduced by adjusting camera angles, distances, and viewpoints during data collection. Fig. 2 (a) provides visual examples of each category, illustrating the challenges posed by different reference conditions in the plant domain.

In SISR, it is common to crop patches from HR images for training randomly. However, in RefSR, corresponding regions with similar content must be cropped from both the HR and Ref images. For example, CUFED5 first randomly crops 160×160 patches from HR images and then selects corresponding patches from Ref images based on predefined correspondence. Similarly, LMR randomly selects a 300×300 patch from the HR image, projects its center to a sparse 3D point cloud, and retrieves Ref patches centered at nearby keypoints. However, these automated cropping strategies are not suitable for plant images. Due to the frequent presence of defocused backgrounds and complex structures in plant scenes, random or keypoint-based cropping often results in uninformative or mismatched patches. Moreover, the significant variations in our paired plant images, such as color, scale, and deformation differences, make accurate automatic correspondence challenging. Therefore, we adopt a manual annotation strategy to carefully select semantically matched regions from image pairs, as illustrated in Fig. 2 (b). Then, we obtain 16,585 patch pairs, which are rescaled into two versions (160×160 and 300×300) to construct the training set (More samples in Appendix K).

4 Our Method

The overview of our method is shown in Fig. 3 (a). Given the LR image I^{LR} and the Ref image I^{Ref}, we aim at generating a high-quality image I^{SR} that possesses texture-rich details conditioned on I^{Ref}. For correspondence matching, we follow C^2-Matching Jiang et al. (2021) and adopt con-

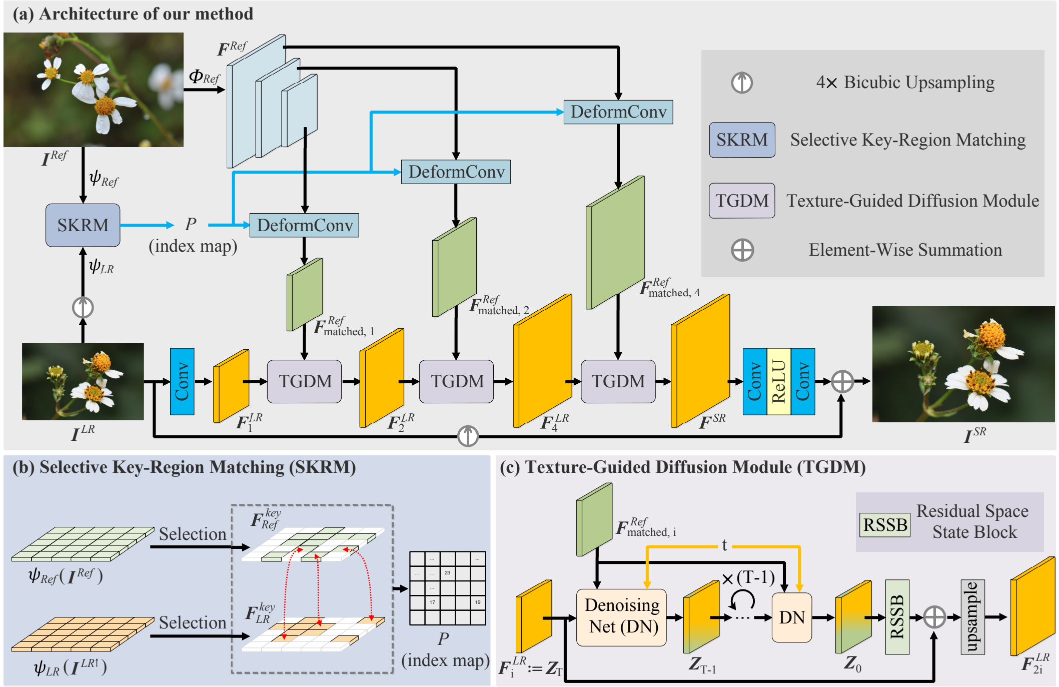

Figure 3: (a) Architecture of our method. (b) Illustration of SKRM. (c) Illustration of TGDM.

trastive learning He et al. (2020) and knowledge distillation Hinton (2015) to train the Ref feature extractor ψ_{Ref} and the LR feature extractor ψ_{LR}. These extractors are used to obtain $\psi_{Ref}(I^{Ref})$ and $\psi_{LR}(I^{LR\uparrow})$ from the Ref and upsampled LR images, respectively. Afterward, our proposed SKRM selectively matches key regions between $\psi_{Ref}(I^{Ref})$ and $\psi_{LR}(I^{LR\uparrow})$ by focusing on informative areas, thereby improving matching efficiency and obtaining the correspondence index map P. To utilize both high-level and low-level information provided by I^{Ref}, following previous works Jiang et al. (2021); Xia et al. (2022); Cao et al. (2022); Zhang et al. (2022), we extract Ref texture features F^{Ref} at different scale levels via encoder Φ_{Ref} Simonyan & Zisserman (2015). At each scale, we perform the deformable convolution networks Dai et al. (2017); Zhu et al. (2019) on F^{Ref} to warp it to match the F^{LR} for later fusion. Finally, our proposed TGDM leverages the diffusion process conditioned on $F^{Ref}_{matched}$ to progressively enhance F^{LR}, thereby enabling more effective multi-scale feature fusion and producing the final SR image I^{SR}. We employ the L1 loss function as the optimization objective during model training.

4.1 Selective Key-Region Matching (SKRM)

Since plant images often contain detailed foregrounds and shallow DoF-induced blurred backgrounds that are easy to reconstruct, explicit matching in such regions is unnecessary. Instead, as illustrated in Fig. 3 (b), we focus on selecting and matching key textured regions. To identify these regions, we introduce a key detail selection indicator. Given a feature map $F \in \mathbb{R}^{H\times W\times C}$ and a sampling ratio $s = 2$, the key detail selection metric $M_F \in \mathbb{R}^{H\times W}$ (values 0 or 1) is obtained through the operation $S(\cdot)$, defined as the absolute difference between the original feature map and its reconstruction via bilinear downsampling and upsampling as:

$$M_F = S(F) = \mathbb{I}(\sum_C \mid F - F_{\downarrow s\uparrow s} \mid > \tau), \tag{1}$$

where τ is the mean plus standard deviation of the absolute differences, $\mathbb{I}(\cdot)$ returns 1 when the input exceeds threshold τ, and 0 otherwise. Considering that the Ref image may also contain blurred background regions, we apply key region selection to the Ref image to enhance matching efficiency with the LR image. Based on Eq. 1, the key detail selection indicators are derived as follows:

$$M_{Ref}, M_{LR} = S(\psi_{Ref}(I^{Ref})), S(\psi_{LR}(I^{LR\uparrow})). \tag{2}$$

Subsequently, the key texture features F_{Ref}^{key} and F_{LR}^{key} are then derived from these indicators as:

$$F_{Ref}^{key} = M_{Ref} * \psi_{Ref}(I^{Ref}), \tag{3}$$

$$F_{LR}^{key} = M_{LR} * \psi_{LR}(I^{LR\uparrow}), \tag{4}$$

Afterward, we get descriptors $d^{Ref} = [k_1, ..., k_m]$ and $d^{LR} = [q_1, ..., q_n]$ from F_{Ref}^{key} and F_{LR}^{key}, respectively. These descriptors are obtained by folding extracted features into patches. Then we find the patch from the patches k_j that is most similar to each LR patch q_i as:

$$P_i = Top1(\frac{q_i}{\|q_i\|} \cdot \frac{k_j}{\|k_j\|}), \tag{5}$$

where $Top1(\cdot)$ is a function and return the most relevant positions P_i.

Then, we use a deformable convolution $DConv(\cdot)$ and the position index map to match the similar textures around every position P_i of F^{LR} as:

$$\begin{aligned} F_{\text{marched},l}^{Ref} &= DConv(F_l^{Ref}, P_i) \\ &= \sum wF_l^{Ref}(P + P_0 + P_i + \Delta p)\Delta m, \end{aligned} \tag{6}$$

where $F_l^{Ref}(l = 1, 2, 4)$ denotes Ref texture features at different scale via encoder Φ_{Ref}, $P_0 \epsilon \{(-1, 1), (-1, 0), ..., (1, 1)\}$, w denotes the convolution kernel weight, Δp and Δm denote the learnable offset and modulation scalar, respectively.

4.2 Texture-Guided Diffusion Module (TGDM)

As shown in Fig. 3 (c), TGDM enhances the LR feature F_l^{LR} by leveraging the matched Ref texture $F_{\text{matched},l}^{Ref}$ as conditional guidance within a diffusion-based refinement framework, enabling a progressive refinement of the LR features with Ref guidance.

We denote the initial LR feature as $F_l^{LR} := Z_T$, which serves as the starting point for the reverse diffusion process. To recover Z_0 from Z_T, we adopt a conditional denoising process Ho et al. (2020); Li et al. (2024b). At each timestep $t \in \{T, T-1, \dots, 1\}$, the Denoising Network (DN) predicts the noise $\hat{\epsilon}_\theta(Z_t, t, F_{\text{matched},l}^{Ref})$ in Z_t conditioned on the matched Ref texture, and each sampling step can be expressed as:

$$q(Z_{t-1}|\hat{Z}_0, Z_t) = \mathcal{N}(Z_{t-1}; \tilde{\mu}_t(\hat{Z}_0, Z_t)\tilde{\beta}_t I), \tag{7}$$

$$\hat{Z}_0 = \frac{1}{\sqrt{\bar{\alpha}_t}} \left(Z_t - \sqrt{1-\bar{\alpha}_t} \cdot \hat{\epsilon}_\theta(Z_t, t, F_{\text{matched},l}^{Ref}) \right), \tag{8}$$

$$\tilde{\mu}_t(\hat{Z}_0, Z_t) = \frac{\sqrt{\bar{\alpha}_{t-1}}\beta_t}{1-\bar{\alpha}_t}\hat{Z}_0 + \frac{\sqrt{\alpha_t}(1-\bar{\alpha}_{t-1})}{1-\bar{\alpha}_t}Z_t, \tag{9}$$

$$\tilde{\beta}_t = \frac{1-\bar{\alpha}_{t-1}}{1-\bar{\alpha}_t}\beta_t, \tag{10}$$

where, α_t and β_t are the forward process coefficients, and $\bar{\alpha}_t = \prod_{s=1}^{t} \alpha_s$. This denoising step is iteratively applied from $t = T$ to $t = 1$, producing the refined latent Z_0 guided by the Ref texture. To further enhance textures feature, we pass Z_0 through a Residual State Space Block (RSSB) Guo et al. (2024) as:

$$\bar{Z}_0 = \text{RSSB}(Z_0). \tag{11}$$

The refined latent $\bar{Z}_0$ is then fused with the original LR feature via residual addition and subsequently upsampled using a sub-pixel convolution layer Shi et al. (2016) as:

$$F_{2l}^{LR} = \text{upsample}(F_l^{LR} + \bar{Z}_0), \quad l = 1, 2. \tag{12}$$

Finally, the enhanced feature F_4^{LR} is used to generate the super-resolved representation by an additional residual connection as:

$$F^{SR} = F_4^{LR} + \bar{Z}_0. \tag{13}$$

TGDM progressively injects Ref-guided textures into the LR representation through the conditional diffusion mechanism, improving feature quality for high-fidelity SR reconstruction.

5 Experiments

5.1 Datasets and Implementation Details

Due to the unavailability of the LMR dataset, we employ CUFED5, DRefSR, and our PlantRSR training datasets for comparative evaluation. All models are trained on 160×160 patches under identical settings to CUFED5 for consistency. The LR images are produced by $4\times$ bicubic downscaling of HR images. All SR results are evaluated using four metrics: PSNR, SSIM Wang et al. (2004), LPIPS Zhang et al. (2018), and DISTS Ding et al. (2020). The PSNR and SSIM values are calculated on the Y channel in YCbCr color space. Besides, we introduce M-PSNR, a variant that measures PSNR only in textured regions using a mask similar to Eq. 1. In our method, the number of T is set to 4. We train our model with 400 epochs using ADAM optimizer (β_1=0.9 and β_2=0.999). The initial learning rate is set to 10^{-4} and decreased by 0.5 after each $100,000$ iteration. We implement experiments using the NVIDIA RTX A6000 GPU.

5.2 Quantitative Evaluation

We compare our method with several SOTA RefSR approaches, including MASA Lu et al. (2021), C^2-Matching Jiang et al. (2021), AMSA Xia et al. (2022), DATSR Cao et al. (2022), RRSR Zhang et al. (2022), MRefSR Zhang et al. (2023), HiTSR Aslahishahri et al. (2024), MCMSR Zheng et al. (2024) and SSMTF Zhou et al. (2025). All comparison methods are trained independently on both the CUFED5 dataset and our PlantRSR dataset. The detailed experimental results are listed in Tab. 1. Our method achieves the best performance across all four metrics on all training datasets. Furthermore, experimental observations reveal that models trained on PlantRSR consistently outperform those trained on CUFED5 and DRefSR. Notably, **Ours** achieves superior performance with only 11.1M parameters, significantly fewer than competitors like RRSR (21.5M) and MRefSR (23.7M). Moreover, all methods exhibit consistent performance improvements when trained on PlantRSR compared to both CUFED5 and DRefSR. Besides, the significantly greater improvement in M-PSNR compared to standard PSNR demonstrates our dataset's enhanced effectiveness for complex plant textures. Experimental results validate method superiority and PlantRSR dataset significance.

5.3 Qualitative Evaluation

We visually compare our method and other methods in Fig. 4. In Fig. 4 (a-c), we present the visual comparison of plant leaf reconstruction. The restoration of leaf venation patterns proves particularly challenging, where our method demonstrates superior texture recovery compared to other approaches. Fig. 4 (d) and (e) present two challenging scenarios involving both color and scale variations. Despite these difficulties, our method achieves superior reconstruction quality compared to other compared approaches. In the complex botanical texture case shown in Fig. 4 (f), our method achieves superior fidelity, while competing methods suffer from noticeable blurring effects. The visual results demonstrate the superiority of our method across various challenging in plant image.

5.4 Ablation Study

About our SKRM. We conduct an ablation study by comparing our SKRM with existing efficient matching methods, including Match & Extraction Module (MEM) Lu et al. (2021) and Coarse-to-Fine Embedded PatchMatch (CFE-PatchMatch) Xia et al. (2022). We calculate GFLOPs for an LR image (400×199) and Ref image (1200×796). As listed in Tab. 2, our SKRM achieves the lowest computational cost (77.86 GFLOPs) while maintaining the best performance. Compared to the exhaustive Enumerated Matching method, SKRM significantly reduces the computation by over 150×. These results (More results in Appendix G) demonstrate the efficiency of our SKRM.

About our TGDM. We conduct an ablation study by comparing our proposed TGDM with existing texture fusion methods, including Dynamic Aggregation (DA) Jiang et al. (2021) and Residual Feature Aggregation (RFA) Cao et al. (2022). As listed in Tab. 3, TGDM achieves the highest performance, outperforming both DA and RFA. To further assess the contribution of the diffusion mechanism in TGDM, we also compare it with a variant that removes the diffusion module. The result shows a performance drop from 38.62 to 38.52 in PSNR, highlighting the importance of the diffusion design. These results validate the effectiveness of our TGDM.

Table 1: Quantitative comparisons of RefSR methods, each independently trained on the CUFED5 Zhang et al. (2019), DRefSR Zhou et al. (2025), and our PlantRSR dataset, with evaluation performed on PlantRSR testing sets. **Bold text** indicates the best results achieved on the respective training datasets.

Method	Param.	Training set	PSNR↑	M-PSRN↑	SSIM↑	LPIPS↓	DISTS↓
MASA	4.0M	CUFED5	38.00	30.46	0.9491	0.1344	0.0863
		DRefSR	38.06	30.54	0.9495	0.1338	0.0859
		PlantRSR	38.24	30.80	0.9510	0.1323	0.0852
C^2-Matching	8.9M	CUFED5	38.23	30.81	0.9508	0.1327	0.0857
		DRefSR	38.27	30.87	0.9509	0.1323	0.0855
		PlantRSR	38.43	31.20	0.9523	0.1300	0.0851
AMSA	9.7M	CUFED5	38.24	30.83	0.9509	0.1324	0.0851
		DRefSR	38.29	30.89	0.9511	0.1321	0.0849
		PlantRSR	38.43	31.23	0.9526	0.1303	0.0842
DATSR	18.0M	CUFED5	38.25	30.81	0.9512	0.1316	0.0842
		DRefSR	38.32	30.91	0.9515	0.1312	0.0839
		PlantRSR	38.48	31.26	0.9527	0.1304	0.0835
RRSR	21.5M	CUFED5	38.26	30.83	0.9510	0.1307	0.0838
		DRefSR	38.31	30.93	0.9513	0.1303	0.0835
		PlantRSR	38.44	31.22	0.9524	0.1299	0.0829
MRefSR	23.7M	CUFED5	38.21	30.76	0.9502	0.1334	0.0862
		DRefSR	38.30	30.91	0.9511	0.1328	0.0859
		PlantRSR	38.42	31.15	0.9516	0.1317	0.0853
HiTSR	13.7M	CUFED5	37.84	30.12	0.9482	0.1399	0.0911
		DRefSR	37.90	30.21	0.9487	0.1390	0.0907
		PlantRSR	38.07	30.49	0.9499	0.1371	0.0900
MCMSR	8.9M	CUFED5	38.26	30.82	0.9510	0.1322	0.0851
		DRefSR	38.30	30.90	0.9516	0.1317	0.0849
		PlantRSR	38.43	31.23	0.9526	0.1302	0.0844
SSMTF	13.9M	CUFED5	38.28	30.86	0.9514	0.1305	0.0834
		DRefSR	38.31	30.92	0.9517	0.1303	0.0833
		PlantRSR	38.49	31.25	0.9528	0.1297	0.0831
Ours	11.1M	CUFED5	**38.40**	**31.14**	**0.9522**	**0.1294**	**0.0828**
		DRefSR	**38.49**	**31.27**	**0.9529**	**0.1292**	**0.0828**
		PlantRSR	**38.62**	**31.53**	**0.9538**	**0.1288**	**0.0826**

Table 2: Ablation study of our SKRM.

Matching Method	GFLOPs	PSNR/SSIM
MEM	620.72	38.36/0.9517
CFE-PatchMatch	124.73	38.58/0.9534
Enumerated Matching	11990.39	**38.62/0.9542**
SKRM	77.86	**38.62**/0.9538

Table 3: Ablation study of our TGDM.

Fusion Method	PSNR/SSIM/M-PSNR
DA	38.43/0.9513/31.18
RFA	38.48/0.9521/31.25
TGDM (w/o diffusion)	38.52/0.9531/31.33
TGDM	**38.62/0.9538/31.53**

About our PlantRSR dataset. To validate the effectiveness of our PlantRSR dataset, we train our method on CUFED5, DRefSR, and PlantRSR datasets, respectively, and evaluate the models on PlantRSR testing dataset. As shown in Fig. 5, our model trained on the PlantRSR dataset consistently outperformed the models trained on CUFED5 and DRefSR across the entire training process, with the highest PSNR of 38.62 dB compared to 38.40 dB and 38.50 dB. This quantitative improvement demonstrates that our PlantRSR dataset significantly outperforms existing CUFED5 and DRefSR datasets when handling complex botanical textures. Besides, as shown in Fig. 6 (a), the model trained on the PlantRSR dataset better leverages Ref image to recover fine textures, such as plant trichomes. Fig. 6 (b) exhibits that our dataset achieves superior recovery of irregular floral textures. These results substantiate the effectiveness of our PlantRSR dataset.

About comparisons of other testing datasets. To further demonstrate the effectiveness of our method, we conduct comparative experiments on the CUFED5 and WR-SR testing datasets commonly compared in RefSR task (See Appendix D for other datasets). All methods are trained on CUFED5 datasets. As listed in Tab. 4, our method consistently outperforms all competitors across both datasets, achieving superior results (See Appendix E for visual comparison).

About sampling steps. We investigate the impact of sampling steps T in our method. As shown in Fig. 7, increasing the number of steps improves the performance, with PSNR gradually saturating after $T = 4$. We also evaluate different texture types by grouping the test images according to their

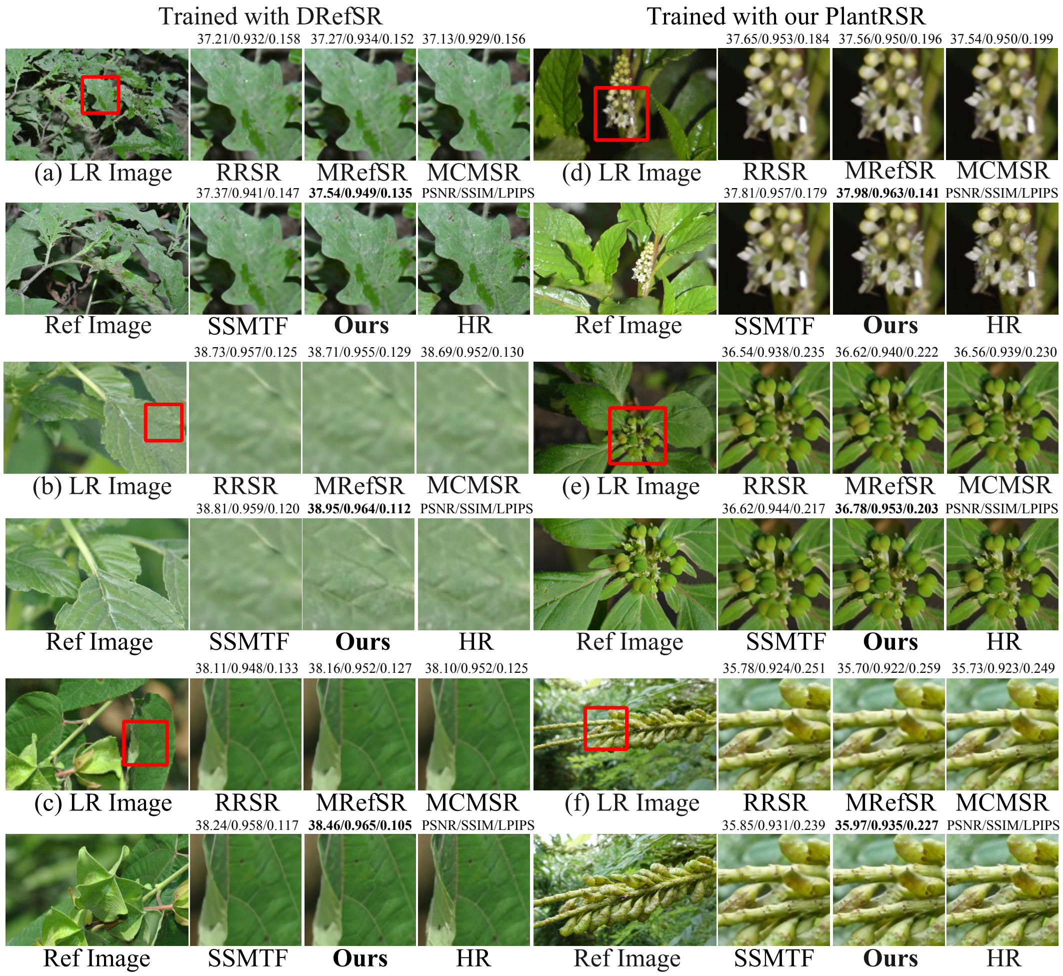

Figure 4: Visual comparison of SOTA RefSR methods, each independently trained on both the DRefSR dataset and our proposed PlantRSR dataset, with evaluation performed on the PlantRSR.

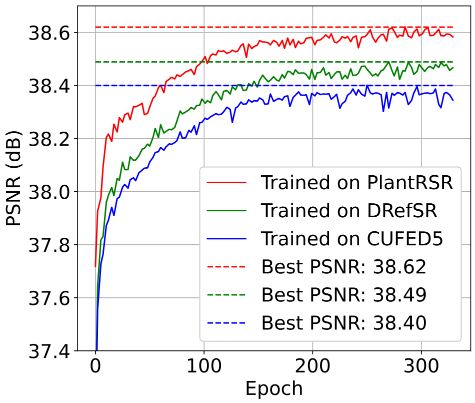

Figure 5: Ablation study comparing model performance when trained on the CUFED5, DRefSR, and our PlantRSR datasets.

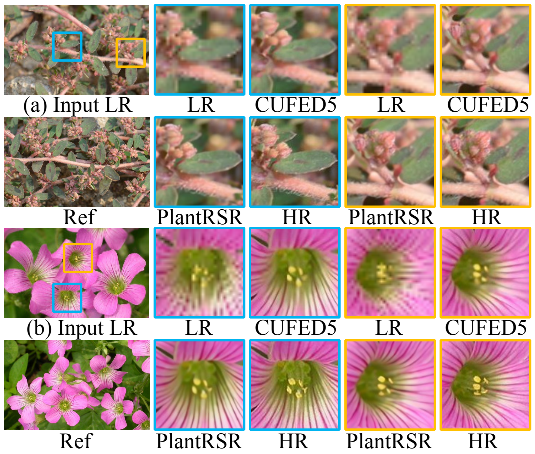

Figure 6: Visual comparison between models trained on CUFED5 and our PlantRSR dataset.

complexity, such as fine veins (25 images) versus thick stems (37 images). As shown in Tab. 5, across all groups, we observed the same trend as in Fig. 7: performance steadily improves when increasing T and saturates at $T = 4$. Importantly, no texture category benefits from larger sampling

Table 4: Quantitative comparisons of SOTA methods on CUFED5 and WR-SR testing datasets, evaluated using PSNR, SSIM, and LPIPS.

Method	CUFED5	WR-SR
RRSR	28.83/0.8563/0.2241	28.41/0.8039/0.2846
MRefSR	28.63/0.8523/0.2281	28.26/0.8012/0.2912
HiTSR	27.08/0.8012/0.2960	28.26/0.8017/0.2958
MCMSR	28.54/0.8490/0.2294	28.34/0.8019/0.2857
SSMTF	28.86/0.8595/0.2202	28.42/0.8056/0.2842
Ours	**28.95/0.8602/0.2184**	**28.51/0.8062/0.2813**

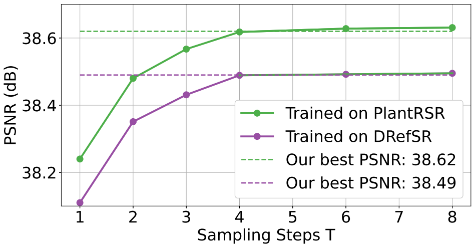

Figure 7: Ablation study of T in TGDM.

steps beyond $T = 4$, confirming that the diffusion refinement behaves consistently across different plant textures. Based on the trade-off between performance and efficiency, we set $T = 4$.

Table 5: About the effects of different sampling steps on different plant textures.

Texture Type	T=1	T=2	T=3	T=4	T=6	T=8
Fine Veins	27.62	27.88	27.95	28.04	28.06	28.07
Thick Stems	36.82	37.07	37.26	37.32	37.33	37.34

About plant categories. We provide a clearer description of plant categories, growth-stage diversity, and real-scene complexity. The dataset covers four major categories of commonly encountered vegetation: crops, wild plants, ornamental plants, and aquatic plants. To improve generalization, data acquisition was conducted over more than one year, covering spring, summer, and autumn, thus naturally capturing early leaf expansion, mid-growth, and mature stages. The overall distribution is listed in the Tab. 6

Table 6: About category of our PlantRSR.

Category	Percentage	Growth-Stage
Crops	10.2%	early, mid, mature
Wild plants	36.3%	early, mid, mature
Ornamental Plants	45.3%	early, mid, mature
Aquatic Plants	8.2%	mid, mature

Table 7: About environment of our PlantRSR.

Environmental Factor	Percentage
Illumination variations	22.7%
Weather effects	9.8%
Background clutter	34.6%
Leaf damage	7.3%

About collection environment. The dataset was deliberately constructed to encompass a wide spectrum of natural environmental changes. Images were captured across different seasons to include diverse factors such as illumination variations, weather effects, background clutter, and instances of leaf damage. A quantitative summary of these conditions and their approximate proportions within the dataset is provided in Tab. 7.

6 Conclusion

In this paper, we address the limitations of existing RefSR datasets and methods in handling natural scenes with complex textures, particularly plant imagery. We introduce **PlantRSR**, a large-scale RefSR dataset containing 16,585 high-quality HR–Ref pairs that capture the diverse and fine-grained characteristics of botanical scenes. To fully exploit this dataset, we propose a novel RefSR framework featuring two key components: a SKRM selectively matches botanical textures to enhance efficiency, and a TGDM for progressive refinement of LR features using Ref-guided diffusion. Extensive experiments demonstrate that our method outperforms existing SOTA approaches in both quantitative metrics and visual quality, highlighting the effectiveness of our design and the value of the PlantRSR dataset for advancing RefSR research in natural and fine-grained scenarios.

7 Acknowledgements

The research is supported by National Science and Technology Major Project (2022ZD0119204), National Science Fund for Distinguished Young Scholars (62125601), and National Natural Science Foundation of China (62576031).

REFERENCES

Masoomeh Aslahishahri, Jordan Ubbens, and Ian Stavness. Hitsr: A hierarchical transformer for reference-based super-resolution. *arXiv preprint arXiv:2408.16959*, 2024.

Jiezhang Cao, Jingyun Liang, Kai Zhang, Yawei Li, Yulun Zhang, Wenguan Wang, and Luc Van Gool. Reference-based image super-resolution with deformable attention transformer. In *European Conference on Computer Vision*, pp. 325–342, 2022.

Qinpeng Cui, Yixuan Liu, Xinyi Zhang, Qiqi Bao, Qingmin Liao, Li Wang, Tian Lu, Zicheng liu, Zhongdao Wang, and Emad Barsoum. Taming diffusion prior for image super-resolution with domain shift sdes. In *Proceedings of the International Conference on Neural Information Processing Systems*, pp. 42765–42797, 2024.

Jifeng Dai, Haozhi Qi, Yuwen Xiong, Yi Li, Guodong Zhang, Han Hu, and Yichen Wei. Deformable convolutional networks. In *Proceedings of the IEEE/CVF International Conference on Computer Vision*, pp. 764–773, 2017.

Tao Dai, Jianrui Cai, Yongbing Zhang, Shu-Tao Xia, and Lei Zhang. Second-order attention network for single image super-resolution. In *Proceedings of the IEEE/CVF Conference on Computer Vision and Pattern Recognition*, pp. 11065–11074, 2019.

Keyan Ding, Kede Ma, Shiqi Wang, and Eero P Simoncelli. Image quality assessment: Unifying structure and texture similarity. *IEEE Transactions on Pattern Analysis and Machine Intelligence*, 44(5):2567–2581, 2020.

Runmin Dong, Shuai Yuan, Bin Luo, Mengxuan Chen, Jinxiao Zhang, Lixian Zhang, Weijia Li, Juepeng Zheng, and Haohuan Fu. Building bridges across spatial and temporal resolutions: Reference-based super-resolution via change priors and conditional diffusion model. In *Proceedings of the IEEE/CVF Conference on Computer Vision and Pattern Recognition*, pp. 27684–27694, 2024.

Hang Guo, Jinmin Li, Tao Dai, Zhihao Ouyang, Xudong Ren, and Shu-Tao Xia. Mambair: A simple baseline for image restoration with state-space model. In *European Conference on Computer Vision*, pp. 222–241, 2024.

Hang Guo, Yong Guo, Yaohua Zha, Yulun Zhang, Wenbo Li, Tao Dai, Shu-Tao Xia, and Yawei Li. Mambairv2: Attentive state space restoration. In *Proceedings of the Computer Vision and Pattern Recognition Conference*, pp. 28124–28133, 2025.

Kaiming He, Xiangyu Zhang, Shaoqing Ren, and Jian Sun. Deep residual learning for image recognition. In *Proceedings of the IEEE Conference on Computer Vision and Pattern Recognition*, pp. 770–778, 2016.

Kaiming He, Haoqi Fan, Yuxin Wu, Saining Xie, and Ross Girshick. Momentum contrast for unsupervised visual representation learning. In *Proceedings of the IEEE/CVF Conference on Computer Vision and Pattern Recognition*, pp. 9729–9738, 2020.

G Hinton. Distilling the knowledge in a neural network. *arXiv preprint arXiv:1503.02531*, 2015.

Jonathan Ho, Ajay Jain, and Pieter Abbeel. Denoising diffusion probabilistic models. *Advances in Neural Information Processing Systems*, 33:6840–6851, 2020.

Yuanfei Huang, Jie Li, Xinbo Gao, Yanting Hu, and Wen Lu. Interpretable detail-fidelity attention network for single image super-resolution. *IEEE Transactions on Image Processing*, 30:2325–2339, 2021.

Yuming Jiang, Kelvin C.K. Chan, Xintao Wang, Chen Change Loy, and Ziwei Liu. Robust reference-based super-resolution via c2-matching. In *Proceedings of the IEEE/CVF Conference on Computer Vision and Pattern Recognition*, pp. 2103–2112, 2021.

Xiangtao Kong, Hengyuan Zhao, Yu Qiao, and Chao Dong. Classsr: A general framework to accelerate super-resolution networks by data characteristic. In *Proceedings of the IEEE/CVF Conference on Computer Vision and Pattern Recognition*, pp. 12016–12025, 2021.

Byeonghun Lee, Hyunmin Cho, Hong Gyu Choi, Soo Min Kang, Iljun Ahn, and Kyong Hwan Jin. Reference-based super-resolution via image-based retrieval-augmented generation diffusion. In *Proceedings of the IEEE/CVF International Conference on Computer Vision*, pp. 10764–10774, 2025.

Guangyuan Li, Chen Rao, Juncheng Mo, Zhanjie Zhang, Wei Xing, and Lei Zhao. Rethinking diffusion model for multi-contrast mri super-resolution. In *Proceedings of the IEEE/CVF Conference on Computer Vision and Pattern Recognition*, pp. 11365–11374, 2024a.

Tianhong Li, Yonglong Tian, He Li, Mingyang Deng, and Kaiming He. Autoregressive image generation without vector quantization. *Advances in Neural Information Processing Systems*, 37: 56424–56445, 2024b.

Zhengqi Li and Noah Snavely. Megadepth: Learning single-view depth prediction from internet photos. In *Proceedings of the IEEE Conference on Computer Vision and Pattern Recognition*, pp. 2041–2050, 2018.

Bee Lim, Sanghyun Son, Heewon Kim, Seungjun Nah, and Kyoung Mu Lee. Enhanced deep residual networks for single image super-resolution. In *Proceedings of the IEEE Conference on Computer Vision and Pattern Recognition Workshops*, pp. 136–144, 2017.

Liying Lu, Wenbo Li, Xin Tao, Jiangbo Lu, and Jiaya Jia. Masa-sr: Matching acceleration and spatial adaptation for reference-based image super-resolution. In *Proceedings of the IEEE/CVF Conference on Computer Vision and Pattern Recognition*, pp. 6368–6377, 2021.

Ben Niu, Weilei Wen, Wenqi Ren, Xiangde Zhang, Lianping Yang, Shuzhen Wang, Kaihao Zhang, Xiaochun Cao, and Haifeng Shen. Single image super-resolution via a holistic attention network. In *European Conference on Computer Vision*, pp. 191–207, 2020.

Ethan Perez, Florian Strub, Harm De Vries, Vincent Dumoulin, and Aaron Courville. Film: Visual reasoning with a general conditioning layer. In *Proceedings of the AAAI Conference on Artificial Intelligence*, volume 32, 2018.

Marco Pesavento, Marco Volino, and Adrian Hilton. Attention-based multi-reference learning for image super-resolution. In *Proceedings of the IEEE/CVF International Conference on Computer Vision*, pp. 14697–14706, 2021.

Wenzhe Shi, Jose Caballero, Ferenc Huszár, Johannes Totz, Andrew P Aitken, Rob Bishop, Daniel Rueckert, and Zehan Wang. Real-time single image and video super-resolution using an efficient sub-pixel convolutional neural network. In *Proceedings of the IEEE Conference on Computer Vision and Pattern Recognition*, pp. 1874–1883, 2016.

Karen Simonyan and Andrew Zisserman. Very deep convolutional networks for large-scale image recognition. In *International Conference on Learning Representations*, 2015.

Haoze Sun, Wenbo Li, Jianzhuang Liu, Haoyu Chen, Renjing Pei, Xueyi Zou, Youliang Yan, and Yujiu Yang. Coser: Bridging image and language for cognitive super-resolution. In *Proceedings of the IEEE/CVF Conference on Computer Vision and Pattern Recognition*, pp. 25868–25878, 2024.

Libin Sun and James Hays. Super-resolution from internet-scale scene matching. In *IEEE International Conference on Computational Photography*, pp. 1–12, 2012.

Radu Timofte, Eirikur Agustsson, Luc Van Gool, Ming-Hsuan Yang, and Lei Zhang. Ntire 2017 challenge on single image super-resolution: Methods and results. In *Proceedings of the IEEE Conference on Computer Vision and Pattern Recognition Workshops*, pp. 114–125, 2017.

Jianyi Wang, Zongsheng Yue, Shangchen Zhou, Kelvin CK Chan, and Chen Change Loy. Exploiting diffusion prior for real-world image super-resolution. *International Journal of Computer Vision*, 132(12):5929–5949, 2024a.

Longguang Wang, Yingqian Wang, Xiaoyu Dong, Qingyu Xu, Jungang Yang, Wei An, and Yulan Guo. Unsupervised degradation representation learning for blind super-resolution. In *Proceedings of the IEEE/CVF Conference on Computer Vision and Pattern Recognition*, pp. 10581–10590, 2021.

Yufei Wang, Zhe Lin, Xiaohui Shen, Radomir Mech, Gavin Miller, and Garrison W Cottrell. Event-specific image importance. In *Proceedings of the IEEE Conference on Computer Vision and Pattern Recognition*, pp. 4810–4819, 2016a.

Yufei Wang, Wenhan Yang, Xinyuan Chen, Yaohui Wang, Lanqing Guo, Lap-Pui Chau, Ziwei Liu, Yu Qiao, Alex C Kot, and Bihan Wen. Sinsr: diffusion-based image super-resolution in a single step. In *Proceedings of the IEEE/CVF Conference on Computer Vision and Pattern Recognition*, pp. 25796–25805, 2024b.

Yuwang Wang, Yebin Liu, Wolfgang Heidrich, and Qionghai Dai. The light field attachment: Turning a dslr into a light field camera using a low budget camera ring. *IEEE Transactions on Visualization and Computer Graphics*, 23(10):2357–2364, 2016b.

Zhou Wang, Alan C Bovik, Hamid R Sheikh, and Eero P Simoncelli. Image quality assessment: from error visibility to structural similarity. *IEEE Transactions on Image Processing*, 13(4):600–612, 2004.

Rongyuan Wu, Lingchen Sun, Zhiyuan Ma, and Lei Zhang. One-step effective diffusion network for real-world image super-resolution. *Advances in Neural Information Processing Systems*, 37: 92529–92553, 2024.

Bin Xia, Yapeng Tian, Yucheng Hang, Wenming Yang, Qingmin Liao, and Jie Zhou. Coarse-to-fine embedded patchmatch and multi-scale dynamic aggregation for reference-based super-resolution. In *Proceedings of the AAAI Conference on Artificial Intelligence*, volume 36, pp. 2768–2776, 2022.

Yanchun Xie, Jimin Xiao, Mingjie Sun, Chao Yao, and Kaizhu Huang. Feature representation matters: End-to-end learning for reference-based image super-resolution. In *European Conference on Computer Vision*, pp. 230–245. Springer, 2020.

Xu Yan, Weibing Zhao, Kun Yuan, Ruimao Zhang, Zhen Li, and Shuguang Cui. Towards content-independent multi-reference super-resolution: Adaptive pattern matching and feature aggregation. In *European Conference on computer vision*, pp. 52–68, 2020.

Fuzhi Yang, Huan Yang, Jianlong Fu, Hongtao Lu, and Baining Guo. Learning texture transformer network for image super-resolution. In *Proceedings of the IEEE/CVF Conference on Computer Vision and Pattern Recognition*, pp. 5791–5800, 2020.

Lin Zhang, Xin Li, Dongliang He, Fu Li, Yili Wang, and Zhaoxiang Zhang. Rrsr: Reciprocal reference-based image super-resolution with progressive feature alignment and selection. In *European Conference on Computer Vision*, pp. 648–664, 2022.

Lin Zhang, Xin Li, Dongliang He, Fu Li, Errui Ding, and Zhaoxiang Zhang. Lmr: a large-scale multi-reference dataset for reference-based super-resolution. In *Proceedings of the IEEE/CVF International Conference on Computer Vision*, pp. 13118–13127, 2023.

Richard Zhang, Phillip Isola, Alexei A Efros, Eli Shechtman, and Oliver Wang. The unreasonable effectiveness of deep features as a perceptual metric. In *Proceedings of the IEEE Conference on Computer Vision and Pattern Recognition*, pp. 586–595, 2018.

Yi Zhang, Qixue Yang, Damon M Chandler, and Xuanqin Mou. Reference-based multi-stage progressive restoration for multi-degraded images. *IEEE Transactions on Image Processing*, 2024.

Zhifei Zhang, Zhaowen Wang, Zhe Lin, and Hairong Qi. Image super-resolution by neural texture transfer. In *Proceedings of the IEEE/CVF Conference on Computer Vision and Pattern Recognition*, pp. 7982–7991, 2019.

Haitian Zheng, Mengqi Ji, Haoqian Wang, Yebin Liu, and Lu Fang. Crossnet: An end-to-end reference-based super resolution network using cross-scale warping. In *Proceedings of the European Conference on Computer Vision*, pp. 88–104, 2018a.

Haitian Zheng, Mengqi Ji, Haoqian Wang, Yebin Liu, and Lu Fang. Crossnet: An end-to-end reference-based super resolution network using cross-scale warping. In *Proceedings of the European Conference on Computer Vision*, pp. 88–104, 2018b.

Hong Zheng, Huabin Heng, Zhiqiang Yan, Kun Zeng, Jinsheng Fang, and Baohua Qiang. A generic multi-correspondence matching framework for reference-based image super-resolution. *IEEE Transactions on Instrumentation and Measurement*, 2024.

Hongyang Zhou, Xiaobin Zhu, Jianqing Zhu, Zheng Han, Shi-Xue Zhang, Jingyan Qin, and Xu-Cheng Yin. Learning correction filter via degradation-adaptive regression for blind single image super-resolution. In *Proceedings of the IEEE/CVF International Conference on Computer Vision*, pp. 12365–12375, 2023.

Hongyang Zhou, Xiaobin Zhu, Jingyan Qin, Yu Xu, Roberto M Cesar-Jr, and Xu-Cheng Yin. Multi-scale texture fusion for reference-based image super-resolution: New dataset and solution. *International Journal of Computer Vision*, pp. 1–22, 2025.

Xizhou Zhu, Han Hu, Stephen Lin, and Jifeng Dai. Deformable convnets v2: More deformable, better results. In *Proceedings of the IEEE/CVF Conference on Computer Vision and Pattern Recognitio*, pp. 9308–9316, 2019.

A The use of large language models

We used Large Language Models to assist or polish the writing, without involving our experiments, figures, or other core contributions.

B Architecture of the Denoising Network (DN)

As shown in Fig. 8, DN is designed to restore the latent feature Z_0 by leveraging both Ref texture features and diffusion timestep. Given the diffusion timestep t, a Embedder maps it into an embedding $t_{\text{emb}} \in \mathbb{R}^d$. This embedding is then fused with the matched Ref features F^{Ref}_{matched} via a simple addition, and passed through a SiLU activation followed by a linear transformation to yield three modulation vectors $a, b, c \in \mathbb{R}^d$:

$$t_{\text{emb}} = \text{Embedder}(t), \tag{14}$$

$$a, b, c = \text{Linear}(\text{SiLU}(F^{Ref}_{\text{matched}} + t_{\text{emb}})). \tag{15}$$

The input latent Z_t is passed by the adaptive layer normalization (AdaLN) Perez et al. (2018); Li et al. (2024b). The result is adaptively modulated using the scale vector a and shift vector b:

$$x_t = a \otimes \text{AdaLN}(Z_t) + b. \tag{16}$$

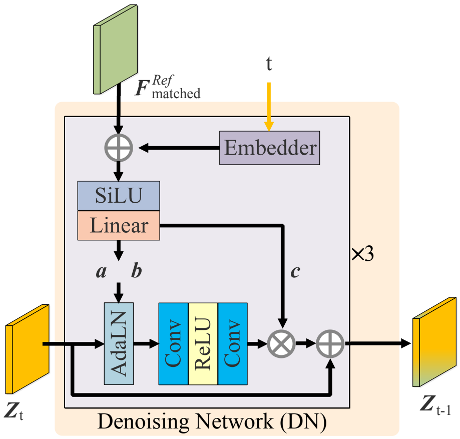

Figure 8: Architecture of Denoising Net.

This modulated feature x_t is further refined by a ResBlock He et al. (2016), whose output is scaled by c and added back to the original input Z_t to obtain the Z_{t-1}:

$$Z_{t-1} = c \otimes ResBlock(x_t) + Z_t. \tag{17}$$

To enhance the representational capacity and further inject Ref information into the denoising process, the above procedure is repeated three times within the DN. This recursive structure enables more effective integration of Ref textures and temporal priors for progressive feature refinement.

C Comparison with the DRefSR Dataset

Although DRefSR contains some plant scenes, its limited scale and diversity are insufficient to address the challenges in plant imagery. As shown in Tab. 8, DRefSR comprises only 1,400 images, whereas our PlantRSR dataset offers 6,134 high-resolution images, with 80% exceeding 4K resolution and exhibiting superior visual quality. Furthermore, PlantRSR provides more comprehensive coverage across five key categories, while DRefSR contains merely a few dozen images in critical dimensions such as color variation, scale diversity, and background complexity—far below the requirements for robust model training. The experimental results in Tab. 1 and Fig 5 further demonstrate the superior effectiveness of our PlantRSR dataset.

Table 8: Analysis of plant image diversity and number in DRefSR and our PlantRSR.

Category	Color	Scale	Rotation	Deformation	Background	All
DRefSR	52 (3.7%)	83 (5.9%)	332 (23.7%)	884 (63.2%)	49 (3.5%)	1,400
PlantRSR	697 (11.4%)	1,142 (18.6%)	1,657 (27.0%)	1,872 (30.5%)	766 (12.5%)	6,134

D Comparison with SOTA methods on other testing datasets

To further demonstrate the effectiveness of our method, we conduct comparative experiments on the Sun80 Sun & Hays (2012) and DRefSR Zhou et al. (2025) testing datasets commonly compared in RefSR task. For fair comparison, all methods are trained on the CUFED5 dataset. As presented in Tab. 9, our method surpasses all competing approaches across all evaluation metrics on both datasets, demonstrating its consistent superiority and effectiveness.

Table 9: Quantitative comparisons of SOTA methods on Sun80 Sun & Hays (2012) and DRefSR Zhou et al. (2025) testing datasets, evaluated using PSNR, SSIM, and LPIPS.

Method	Sun80	DRefSR
RRSR	30.13/0.816/0.303	31.69/0.867/0.280
MRefSR	30.28/0.819/0.301	31.72/0.868/0.279
HiTSR	30.24/0.821/0.293	31.26/0.858/0.290
MCMSR	30.21/0.818/0.300	31.24/0.856/0.294
SSMTF	30.38/**0.824**/0.286	31.75/0.869/0.277
Ours	**30.41/0.824/0.284**	**31.77/0.871/0.272**

E Visual comparison on other testing datasets

To further demonstrate the effectiveness of our method, we conduct comparative experiments on the CUFED5 Zhang et al. (2019) and WR-SR Jiang et al. (2021) testing datasets commonly compared in RefSR task. All methods are trained on CUFED5 datasets. As shown in Fig. 11, our method demonstrates superior visual reconstruction performance compared to other approaches across both datasets.

Table 10: Performance in terms of different similarity levels on CUFED5 dataset. All methods trained on CUFED5 dataset.

Similarity Levels	DATSR	RRSR	HiTSR	MCMSR	SSMTF	Ours
L1	28.50/0.850	28.63/0.851	26.82/0.797	28.54/0.849	28.76/0.854	**28.86/0.855**
L2	27.47/0.820	27.67/0.821	26.68/0.785	27.54/0.808	27.71/0.824	**27.81/0.826**
L3	27.22/0.811	27.41/0.813	26.56/0.783	27.27/0.810	27.46/0.816	**27.58/0.819**
L4	26.96/0.803	27.15/0.804	26.43/0.781	27.03/0.801	27.19/0.807	**27.29/0.809**
LR	25.75/0.754	26.53/0.784	26.53/0.782	26.41/0.782	26.68/0.791	**26.70/0.791**
Average	27.18/0.808	27.47/0.815	26.60/0.786	27.36/0.810	27.56/0.818	**27.65/0.820**

F About similarity of Ref image

To evaluate the impact of reference images with varying similarity levels on model performance, which provides four Ref images (L1–L4) with decreasing similarity to the LR image, where L1 is the most similar and L4 the least. We evaluate our method using all similarity levels, including the LR image itself as a Ref when similar ones are unavailable. As listed in Tab. 10, our method consistently outperforms SOTA approaches across all levels, even when using only the LR image as a Ref, demonstrating its robustness and generalization ability.

Table 11: Computational cost and memory usage of different methods.

Method	Param.	Runtime	Memory
RRSR	21.5M	1.496s	13.3G
MRefSR	23.7M	0.774s	14.1G
HiTSR	13.7M	0.843s	8.5G
MCMSR	8.9M	0.681s	8.6G
SSMTF	13.9M	1.435s	15.2G
Ours	11.1M	1.116s	11.4G

G COMPUTATIONAL COST AND MEMORY USAGE

To assess the practicality of our method, we compare the runtime and memory consumption with several recent RefSR methods in Tab. 11. All values are measured using an LR image of size 300×200 and a Ref image of size 1200×800. As listed in Tab. 11, while our method does not achieve the lowest runtime or memory usage, it maintains a reasonable balance between efficiency and performance. Although we adopt a diffusion process, the network structure is lightweight, consisting of only three ResBlocks, and the sampling steps during inference are limited to four. Therefore, the computational and time costs are not as significant. In addition, our SKRM module effectively reduces the time required for Ref texture matching, resulting in competitive overall runtime and memory usage.

Table 12: Comparison with diffusion-based methods on PlantRSR dataset.

Method	PSNR	SSIM	LPIPS	DISTS
SinSR Wang et al. (2024b)	31.60	0.8580	0.1886	0.1449
DoSSR Cui et al. (2024)	30.82	0.8600	0.2192	0.2091
StableSR Wang et al. (2024a)	31.21	0.8774	0.2011	0.1930
OSEDiff Wu et al. (2024)	32.22	0.8975	0.1602	0.1312
Ours	38.62	0.9538	0.1288	0.0826

H COMPARISON WITH DIFFUSION-BASED METHODS

We conduct comparative experiments with diffusion-based methods, as listed in Tab. 12. It should be noted that this comparison may present certain inequities and is primarily intended for experimental reference. These diffusion-based approaches are built upon generative diffusion models, while our method is trained using pixel-wise losses (e.g., L1 loss). Furthermore, the diffusion architectures are substantially larger and more complex, whereas our method adopts a lightweight design comprising only three ResBlocks. Additionally, these comparative methods do not utilize reference images, which places them at a inherent disadvantage in the reference-based super-resolution setting.

Table 13: The user study. Compared to other methods, over 90% users prefer our results.

Ours vs. RRSR	Ours vs. MRefSR	Ours vs. MCMSR	Ours vs SSMTF
93%	95.3%	93%	90.7%

I USER STUDY

To further validate the qualitative superiority, as listed in the table below, we conduct a user study involving 43 participants to compare the visual quality of our method against several methods on our PlantRSR dataset, including RRSR, MRefSR, HiTSR, MCMSR, and SSMTF. In each comparison, participants are shown image pairs, with one generated by Ours, and are asked to select the image with better visual quality. According to the table below, over 90% of participants favor the results of our method over the other approaches.

J Limitation

While this work advances RefSR for plant imagery, two key limitations should be noted. First, hardware constraints force suboptimal downsampling of our high-resolution dataset (80% $>$ 4K, range 2K-8K), preventing full utilization of the available image detail. Second, performance degrades when processing dissimilar Ref images, as the current matching mechanism lacks adaptability to low-similarity scenarios. These limitations point to important research directions: developing memory-efficient architectures for ultra-high-resolution processing and designing more selective Ref utilization strategies. Addressing these challenges would significantly enhance the practical applicability of plant image SR.

K Partial Samples from the PlantRSR Dataset

As shown in Fig. 9 and Fig. 10, our PlantRSR dataset contains meticulously annotated samples spanning multiple plant categories with rich textures. The manual annotation process specifically captures challenging plant scenarios, ensuring dataset quality for advanced botanical studies.

L Ethics Statement

Our proposed dataset focuses on plant scene imagery, and our method is designed for reference-based image super-resolution. Neither the dataset nor the proposed method involves human subjects, personal data, or sensitive information. The dataset was constructed from images captured by our team and does not infringe upon the interests of any individuals or communities. All experimental results are derived from either publicly available datasets or our constructed dataset. We do not foresee any direct social harms arising from this research.

M Reproducibility Statement

Our codes are released at: `https://github.com/edbca/PlantRSR`. The generation process of our PlantRSR dataset is presented in Section 3. The training details of our proposed method are described in Section 5.1 of the main text. More details of denoising network are given in Appendix B, while Appendix K provides more samples from the PlantRSR training and testing datasets. The usage of large language models is discussed in Appendix A.

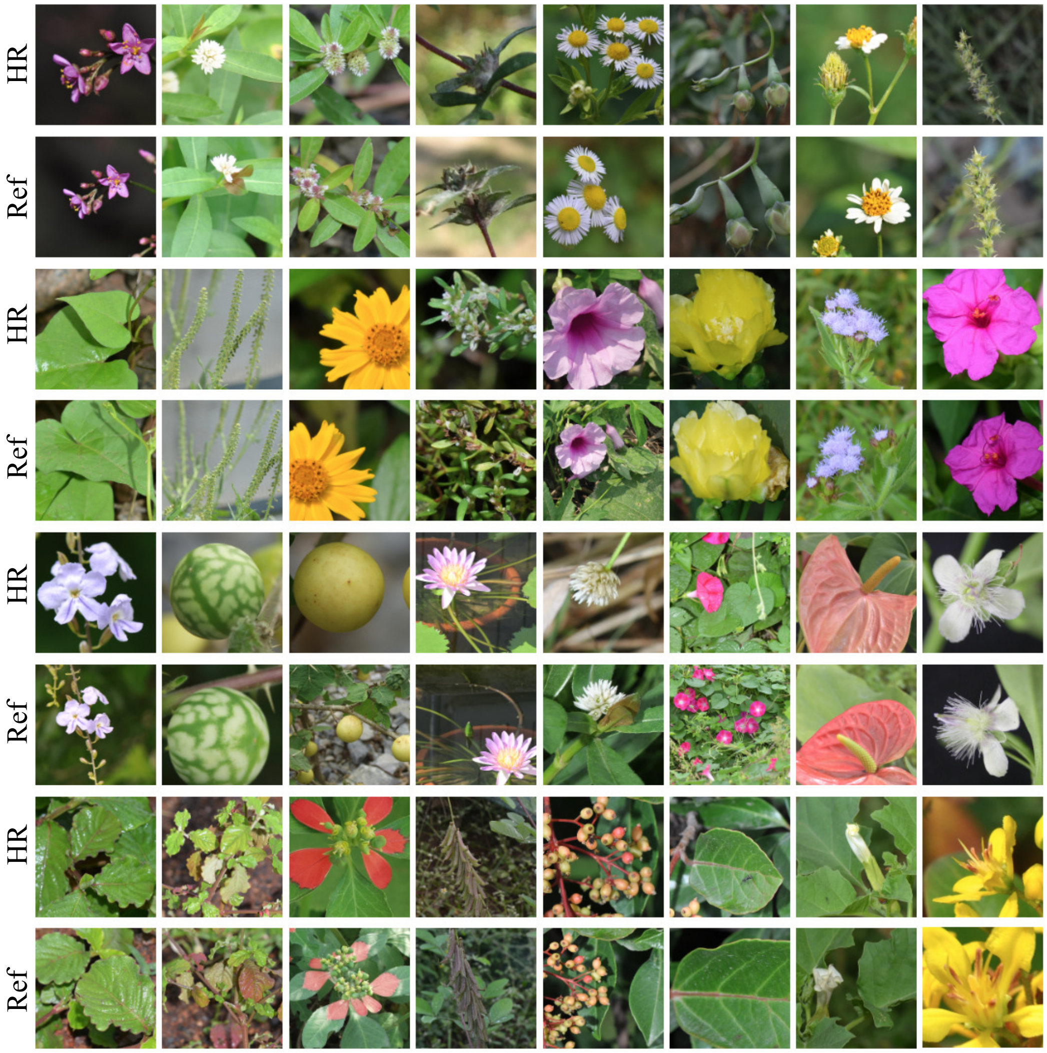

Figure 9: Partial Samples of our PlantRSR training dataset.

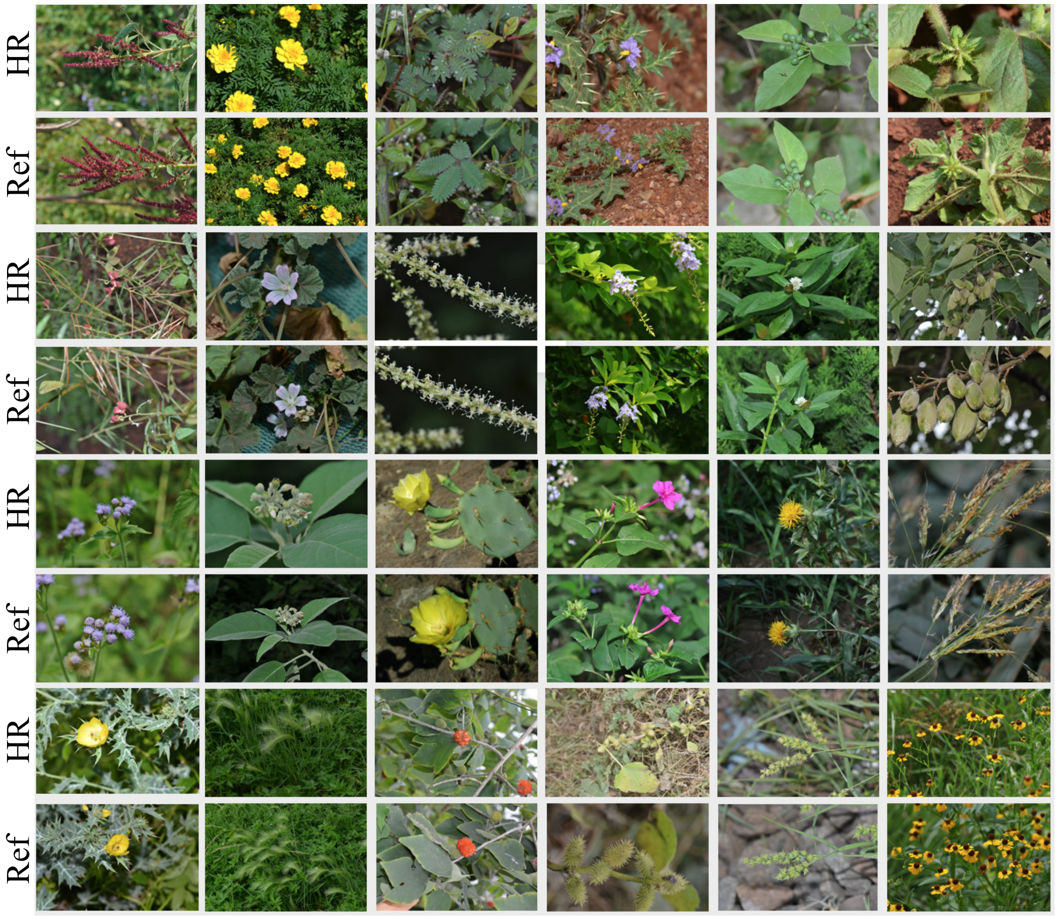

Figure 10: Partial Samples of our PlantRSR testing dataset.

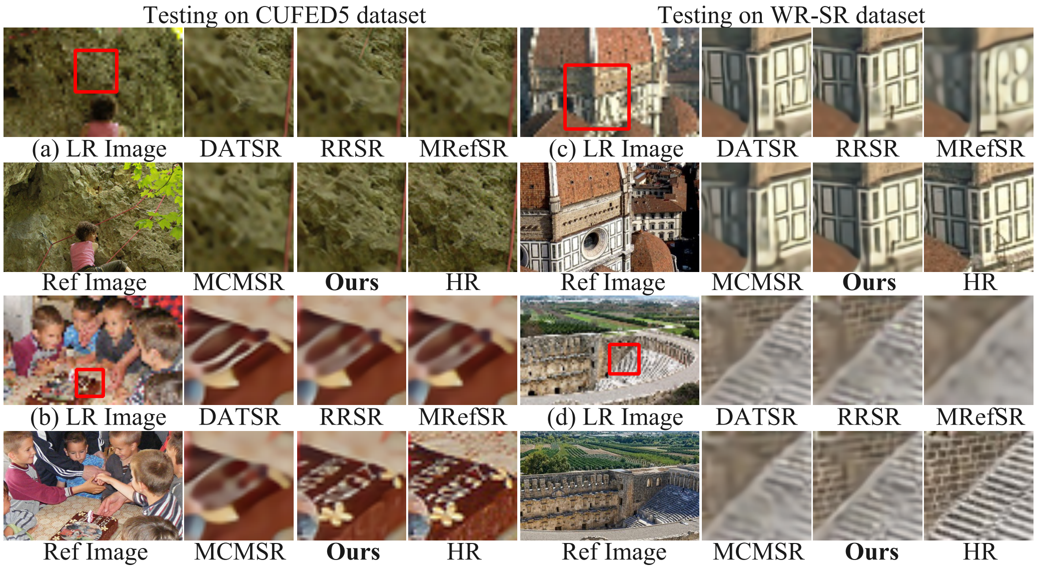

Figure 11: Visual comparison with SOTA methods on CUFED5 and WR-SR datasets.